Sensors & Transducers, Vol. 176, Issue 8, August 2014, pp. 27-37

Sensors & Transducers

http://www.sensorsportal.com

Sensing Property Modeling for the Novel Horizontal-vertical Composite Underground Displacement Sensor

[1] Nanying Shentu, [2] Guohua Qiu, [1] Xiong Li, [1] Renyuan Tong, [1, *] Qing Li
[1] College of Mechatronics Engineering, China Jiliang University, Hangzhou, 310018, P. R. China
[2] College of Information Engineering, China Jiliang University, Hangzhou, 310018, P. R. China
[*] Tel.: +86 571 86914543, fax: +86 571 86914547
[*] E-mail: lq_cjlu@163.com

Received: 2 April 2014 /Accepted: 31 July 2014 /Published: 31 August 2014

Abstract: Due to invisibility and complexity of the underground displacement monitoring, there exit few practical monitoring sensors capable of monitoring the underground horizontal and vertical displacements simultaneously. A novel electromagnetic underground displacement sensor able to monitor both the horizontal and the vertical displacements was proposed in our previous studies and abbreviated as the H-V type sensor. Through comprehensive application of Hall sensing mechanism analysis, 3D magnetic field distribution solution to the permanent magnet, and multidimensional numerical integration method, a model called the Equivalent Magnetic Charge-Numerical Integration Model (EMC-NI) is presented in this paper and serves as the H-V type sensor's Hall voltage measurement model. This model can quantitatively evaluate the complicated relationship among the sensor's Hall voltage output, its measuring parameters (underground horizontal displacement, vertical displacement and tilt angle at different depth within the monitored soil rock mass) and morphological parameters (geometry, shape and property parameters for the sensor units). Comprehensive studies and comparisons have conducted between the experimentally measured and EMC-NI modeled Hall voltage under counterpart conditions, through which not only the model's modeling effectiveness and calculation accuracy are objectively evaluated, but also some valuable theoretical support is provided for the sensor' sensing properties evaluation, design optimization, and subsequent study of displacement parameter inversion approach.

Keywords: Computational modeling, Hall effect, Horizontal displacement, Permanent magnet, Underground displacement sensor, Vertical displacement.

1. Introduction

Underground displacement monitoring is an important means and research hotspot in geological disaster prediction and geotechnical engineering project safety evaluation [1-3]. It can go deep into the soil and rock mass to conduct dynamic monitoring of the geological parameters such as horizontal displacement, vertical displacement and tilt direction at varied underground depth, thus can quantitatively determine the sliding surface (zone) and deformation range, study the deformation mechanism, disaster situation and development trend, and forecast and alleviate the geological disaster. However, due to suddenness and invisibility of the monitoring object, and terribleness and complexity of the monitoring conditions, the underground displacement monitoring technology is slowly developed. Up to now there exist only a few practicable monitoring instruments such as inclinometer, settlement gauge, extensometer

and TDR [4-7], with such drawbacks as poor accuracy, high cost, low automation or difficulty to accurately measure the underground displacement.

In previous studies [8], we proposed a novel electromagnetic horizontal and vertical composite underground displacement sensor (abbreviated as the H-V type sensor). It can measure the underground horizontal displacement, vertical displacement and tilt angle simultaneously from ground till the underlying fixed rock. It is mainly characterized by integration of such sensing mechanisms as the electromagnetic induction, Hall effect and gravity-based inclination measuring. Compared to the conventional underground displacement monitoring methods such as inclinometer and extensometer, it has such advantages as simple principle and structure, time and cost saving, relatively high sensitivity, remote and automatic monitor capability and is applicable for such projects as translational landslide, collapse, ground subsidence and soft soil foundation that require for underground displacement monitoring both in horizontal and vertical directions [9-11].

As Fig. 1 shows, the sensor is mainly composed of two adjacent integrated sensing units with identical structure, i.e., the outer wall is an air-cored solenoid, and the cylindrical inner wall is embedded with the underground displacement measuring integrated circuit PCB board. During working process, the lower sensor unit is functioned as a signal excitation unit and called as Solenoid I, and the upper sensor unit as a signal receiving unit and called as Solenoid II. Along with movement of the surrounding rock and soil mass, a relative horizontal displacement ΔX, vertical displacement ΔZ and/or inclination θ_0 are freely occurred between Solenoid I and II, making the mutual inductance voltage U_o and Hall voltage U_H generated on Solenoid II varied simultaneously. Meanwhile, the sensor's built-in tilt measuring integrated circuit can directly measure the relative axially tilt angle θ_0 between these two sensor units. So the sensor can reversely derivate the measuring underground horizontal displacement ΔX and vertical displacement ΔZ according to output variations of mutual inductance voltage U_o, Hall voltage U_H and tilt angle θ_0.

Corresponding to it, the sensor has two theoretical modeling goals. First, to establish a mutual inductance voltage measuring model suitable for SCM hardware implementation with acceptable calculation precision and efficiency, to qualitatively characterize the functional relationship among the said sensor's mutual inductance voltage output U_o, the measuring parameters (i.e., the relative horizontal displacement ΔX, relative vertical displacement ΔZ, and relative tilt angle θ_0 between Solenoid I and II), and the geometry parameters of two sensor units (e.g., the two solenoids' diameter d, length h, and coil turns w, and the initial vertical distance Z_0 and horizontal distance X_0 between them), that is, to solve the general expression (1). Second, to establish a Hall voltage measuring model suitable for SCM hardware implementation with high calculation precision and efficiency, to qualitatively depict the complicated relationship among the sensor's Hall voltage output U_H, the measuring parameters (i.e., ΔX, ΔZ, and θ_0), and the geometry and property parameters of two sensor units (e.g., the two solenoids' diameter d, length h, and the initial vertical distance Z_0 and horizontal distance X_0 between them, the permanent magnet's diameter D, height H, and sensing property parameter R'_H), that is, to evaluate the general expression (2) by way of theoretical modeling.

$$U_o = (U_i / L_1) f_2(\Delta X, \Delta Z, \theta_0; Z_0, X_0, d, h, w) \quad (1)$$

$$U_H = R'_H f_3(\Delta X, \Delta Z, \theta_0; X_0, Z_0, d, h, D, H) \quad (2)$$

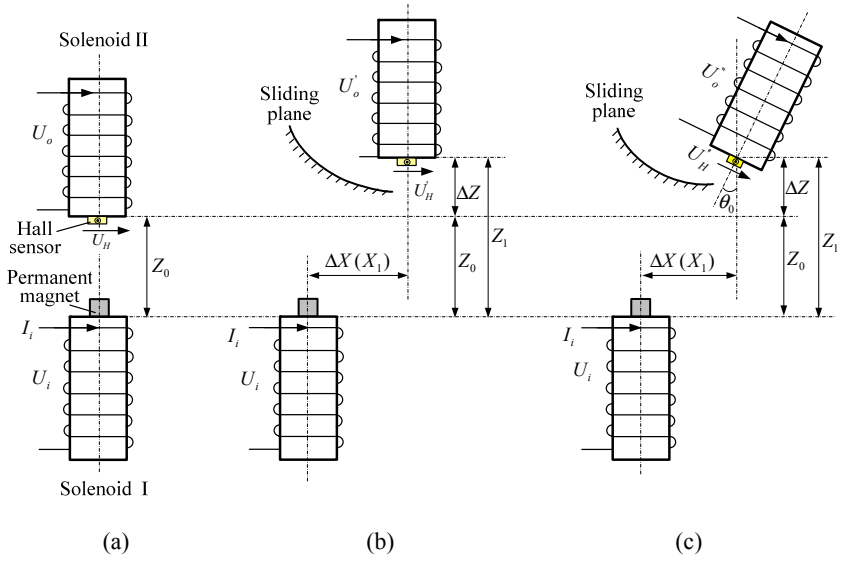

Fig. 1. Schematic diagram of the H-V type underground displacement sensor. (a) Initial coaxial arrangement; (b) relative horizontal displacement ΔX and relative vertical displacement ΔZ occurred; (c) ΔX, ΔZ and θ_0 occurred.

In our previous studies on the H-V type sensor [8], a mutual inductance voltage measurement model called the Numerical Integration-based Equivalent Loop Model (NIELA) was advocated and verified to be a quite accurate and efficient model in characterizing the H-V sensor's mutual inductance properties, thus the theoretical modeling goal 1 has well achieved.

This paper is targeted to further complete the theory modeling goal 2 on basis of the above study. Therefore, through comprehensive application of Hall sensing mechanism analysis, 3D magnetic field solution to the permanent magnet, and the multidimensional numerical calculation technology, a theoretical model named the Equivalent Magnetic Charge-Numerical Integration Model (EMC-NI) is advocated as the sensor's Hall voltage measurement model, which provides a quantitative description of the sophisticated relationship as general expression (2) depicted. Furthermore, a series of comparative studies are conducted between experimental results and modeling simulations to verify the modeling efficiency and accuracy of EMC-NI in depicting of the sensing properties. On such basis, combination of NIELA and EMC-NI models form the H-V type sensor's underground displacement measuring theoretical models.

2. Hall Voltage Measurement Modeling

As illustrated in Fig. 1, for the H-V type sensor, the upper surface center of Solenoid I is fixed with a small cylindrical permanent magnet, and the lower surface center of Solenoid II is fitted with a high sensitivity linear Hall sensor, which is nearby equipped with a compact Hall voltage measuring integrated circuit and its output Hall voltage is denoted by U_H. Therefore, in order to quantitatively and accurately describe the functional relationship concerning the sensor's Hall voltage output U_H varied with change of the relative horizontal displacement ΔX, vertical displacement ΔZ and tilt angle θ_0, a series of theoretical studies are required. Firstly, the 3D spatial distribution of magnetic field generated by the cylindrical permanent magnet need be derived. Secondly, the relative geometrical position between the Hall sensor and permanent magnet and their own geometry should be analyzed. Thirdly, the sensing property of Hall sensor SS941A and I/O property of Hall voltage measuring circuit require to study. After an in-depth theoretical exploration to the above influential factors, we have proposed a Hall voltage measuring model with quite high efficiency and accuracy and suitable for MCU hardware realization. Referred to as the Equivalent Magnetic Charge-Numerical Integration Model (EMC-NI), it is mainly modeled by 3 steps:

Step 1: Derivation of 3D magnetic field solution to the cylindrical permanent magnet by mixing the equivalent magnetic charge model with multidimensional numerical integral technology.

Step 2: Calculation of the effective component of magnetic field that exerted by the permanent magnet on the Hall sensor.

Step 3: Establishment of a complete Hall voltage measuring model by further incorporating analysis of the sensing characteristics of Hall sensor and I/O properties of Hall voltage measuring circuit.

2.1. 3D Magnetic Field of Permanent Magnet

With the wide application of permanent magnetic materials and development of magnet preparation technology, computation of magnetic field produced by the permanent magnet is more widely studied both at home and abroad. At present, apart from the direct formula derivation method starting from the basic electromagnetic field theory to deduce the magnetic field distribution of permanent magnets, there are mainly three models for the magnetic field evaluation: the magnetic dipole model, the equivalent magnetic model, and the equivalent current model [12-14].

In the magnetic dipole mode, the permanent magnet is modeled as a magnetic dipole, ignoring its shape and size. So this model is effective only when the permanent magnet size is far smaller than the distance from the source point to the detect point. In case of our proposed sensor, to make sure that the Hall voltage signal is detectable even when quite a large relative horizontal or/and vertical displacement has occurred between Solenoid I and II, the initial vertical distance Z_0 between them cannot be too large (generally $Z_0 \leq 45$ mm is required) while the permanent magnet size cannot be too small. For the experiments conducted below the material and size of the permanent magnet are shown in Table 1. Under such conditions, it's hard to guarantee the distance from the detect point (Hall sensor) to the source point (permanent magnet) is much larger than the size of permanent magnet. So the magnetic dipole model is unsuitable for establishment of 3D permanent magnetic field in this paper.

Table 1. Geometry and Material of Permanent Magnet.

Magnet type	Diameter (mm)	Height (mm)	Rema-nence (T)	Coercive force (kA/m)
NdFeBN35	5.6	18	1.21	907

The equivalent current model and equivalent magnetic charge model are two equivalent physical models. Both starting from the basic electromagnetic field equations - Maxwell equations and exploring deep into the electromagnetic constitutive relations and magnetic media interface conditions, these two models have modeled the permanent magnet to distributions of the equivalent electric currents and equivalent magnetic charges respectively following

certain electromagnetic rules, and indirectly obtained their 3D magnetic field solutions by superposition of these equivalent currents and magnetic charges generated in the surrounding space respectively.

Generally speaking, starting from the view of magnetized electric charge, the equivalent current mode hypothesizes that there are magnetized currents existing both inside and on the boundary of permanent magnet with current density of $\mathbf{J}_m$ and $\mathbf{J}_{sm}$ respectively, and superposition of these equivalent currents forms the spatial magnetic field of permanent magnet. Meanwhile, the equivalent magnetic charge mode assumes the permanent magnet to be a collection of equivalent magnetic charges with the magnetic charge surface density ρ_m and volume density ρ_{sm} respectively, and superposition of these equivalent magnetic charges through surface integral and volume integral reproduces the magnet's magnetic field.

By comparison, the magnetic charge volume density ρ_m and surface density ρ_{sm} hypothesized in the equivalent magnetic charge model are scalars, and the current volume density $\mathbf{J}_m$ and surface density $\mathbf{J}_{sm}$ assumed in the equivalent current model are vectors composing of three components. So applying the equivalent current model to evaluate the 3D magnetic field might be more complex and time consuming compared to the equivalent magnetic charge mode under the same shape, size and solving domain for the permanent magnet.

After a comprehensive comparison among these three models, a semi-analytic calculation approach combing the equivalent magnetic charge model with double numerical integration has been proposed in this paper to model the 3D magnetic field distribution produced by the H-V type sensor's built-in cylindrical permanent magnet.

Fig. 2 shows the studied cylindrical permanent magnet with radius R, height D, and uniform magnetization intensity $\mathbf{M}_c$ along its axial direction. Choose the magnet's lower surface center as the origin and the symmetry axis as z-axis to establish the Cartesian coordinate and cylindrical coordinate simultaneously. It is noted that according to the equivalent magnetic charge model theory [14], when the magnet is considered to be uniformly magnetized, the magnet's magnetic charge volume density ρ_m is equivalent to zero and the magnetic surface charges exist only on the magnet's boundary with magnetic charge surface density ρ_{sm}, so the magnetic field produced by the magnet at detect point P can be solved by

$$\mathbf{B} = \frac{1}{4\pi}\int_S \frac{\rho_{sm}\mathbf{R}^0}{R^2} dS \,, \tag{3}$$

where $\boldsymbol{R}^0$ is the unit direction vector from the source point to detect point and R is the distance between them, S is the closed integration surface enclosed by the permanent magnet.

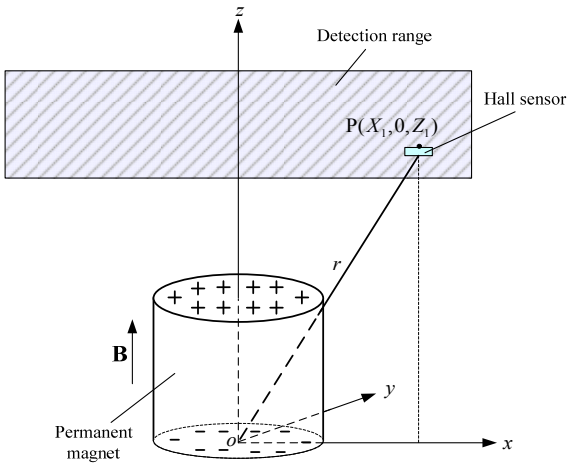

Fig. 2. Schematic diagram of Hall voltage measurement model.

Furthermore, due to the axial magnetization, the magnetic surface charges exist only on the upper and lower surface of the cylindrical magnet with the same magnetic charge density σ_{sm} and the opposite polarity. So expression (3) can be simplified as

$$\mathbf{B} = \mathbf{B}_+ + \mathbf{B}_- = \frac{\sigma_{sm}}{4\pi}\left[\int_{S+}\frac{\mathbf{R}_+}{R_+^3}dS - \frac{1}{4\pi}\int_{S-}\frac{\mathbf{R}_-}{R_-^3}dS\right], \tag{4}$$

where **B**+ and **B**- are the magnetic flux density induced by the positive and negative magnetic charges respectively, S+ and S- are the source integration domains for the positive and negative magnetic charges respectively, **R**+ and **R**- are the distance vector from the source point regarding the positive and negative magnetic charges respectively to the field point, R+ and R- are their corresponding distances.

As shown in Fig. 2, under the cylindrical coordinate an arbitrary source point on the upper surface and lower surface can be represented as $\mathrm{Q}_+(\rho',\varphi',H)$ and $\mathrm{Q}_-(\rho',\varphi',0)$ respectively. An arbitrary field point above the magnet can be denoted as $\mathrm{P}(\rho,\varphi,z)$ that satisfies $z > H$, analysis of the geometric relationship between the source and field points gives

$$\begin{aligned}\mathbf{R}_+ &= (\rho\cos\varphi - \rho'\cos\varphi')\mathbf{e}_x \\ &\quad + (\rho\sin\varphi - \rho'\sin\varphi')\mathbf{e}_y + (z-H)\mathbf{e}_z\end{aligned} \tag{5}$$

$$\begin{aligned}\mathbf{R}_- &= (\rho\cos\varphi - \rho'\cos\varphi')\mathbf{e}_x \\ &\quad + (\rho\sin\varphi - \rho'\sin\varphi')\mathbf{e}_y + z\mathbf{e}_z\end{aligned} \tag{6}$$

$$R_+ = \sqrt{\rho^2 + \rho'^2 + (z-H)^2 - 2\rho\rho'\cos(\varphi-\varphi')} \tag{7}$$

$$R_- = \sqrt{\rho^2 + \rho'^2 + z^2 - 2\rho\rho'\cos(\varphi-\varphi')} \tag{8}$$

substitute (5)-(8) into (4) with simplification, we get

$$B_+ = \frac{B_r}{4\pi}\int_0^{2\pi} d\varphi' \int_0^{D/2} \rho' d\rho' \cdot \frac{(\rho\cos\varphi - \rho'\cos\varphi')\mathbf{e}_x + (\rho\sin\varphi - \rho'\sin\varphi')\mathbf{e}_y + (z-H)\mathbf{e}_z}{\left[\rho^2 + \rho'^2 + (z-H)^2 - 2\rho\rho'\cos(\varphi - \varphi')\right]^{3/2}} \quad (9)$$

More specifically,

$$B_+ = B_{+x}\mathbf{e}_x + B_{+y}\mathbf{e}_y + B_z\mathbf{e}_z, \quad (10)$$

where

$$B_{+x} = \frac{B_r}{4\pi}\int_0^{2\pi} d\varphi' \int_0^{D/2} \cdot \frac{\rho'(\rho\cos\varphi - \rho'\cos\varphi')d\rho'}{\left[\rho^2 + \rho'^2 + (z-H)^2 - 2\rho\rho'\cos(\varphi - \varphi')\right]^{3/2}} \quad (11)$$

$$B_{+y} = \frac{B_r}{4\pi\mu}\int_0^{2\pi} d\varphi' \int_0^{D/2} \cdot \frac{\rho'(\rho\sin\varphi - \rho'\sin\varphi')d\rho'}{\left[\rho'^2 + \rho^2 + (z-H)^2 - 2\rho\rho'\cos(\varphi - \varphi')\right]^{3/2}} \quad (12)$$

$$B_{+z} = \frac{B_r}{4\pi\mu}\int_0^{2\pi} d\varphi' \int_0^{D/2} \cdot \frac{\rho'(z-H)d\rho'}{\left[\rho'^2 + \rho^2 + (z-H)^2 - 2\rho\rho'\cos(\varphi - \varphi')\right]^{3/2}} \quad (13)$$

At this time, it's very difficult to further obtain the analytical expressions for Eqs. (11)-(13). The application of electromagnetic numerical calculation methods [15, 16] for further solution is more reliable and less complex.

As one part of the underground displacement sensor, the Hall voltage measurement model needs to convert into a functional module of executable program and transplant into SCM by programming, so the executive algorithm for the Hall voltage measurement model requires relatively simple operation, high calculation speed and qualified precision. The two-dimensional (2-D) Newton-Cotes integral algorithm is selected to further evaluation of (11)-(13). This algorithm has relatively simple calculation process and high measuring precision and is suitable for hardware implement. Some related 2-D Newton-Cotes integral formula is given as follows.

Assume that the 2-D integral function $f(x, y)$ has a rectangular integral domain expressed as $D_2=[X_1, X_2] \times [Y_1, Y_2]$ and exits 6-order continuous partial derivatives $\frac{\partial^6 f}{\partial x^6}$ and $\frac{\partial^6 f}{\partial y^6}$, then the integral area $[X_1, X_2]$ and $[Y_1, Y_2]$ can be divided into $4m$ and $4n$ uniform intervals respectively with the following interval steps

$$h_x = \frac{X_2 - X_1}{4m}, \; h_y = \frac{Y_2 - Y_1}{4n} \quad (14)$$

The corresponding uniform interval nodes for area $[X_1, X_2]$ and $[Y_1, Y_2]$ can be expressed as

$$\begin{aligned} x_i &= X_1 + ih_x, \quad i = 0,1,...,4m \\ y_j &= Y_1 + jh_y, \quad j = 0,1,...,4n \end{aligned} \quad (15)$$

After a series of derivation and simplification, the 2-D composite Newton-Cotes numerical integration formula can be finally written as

$$\begin{aligned} I &= \int_{X_1}^{X_2}\int_{Y_1}^{Y_2} f(x,y)dxdy \\ &= (2/45)^2 h_x h_y \sum_{i=0}^{4m}\sum_{j=0}^{4n} C_i C_j f(x_i, y_j), \end{aligned} \quad (16)$$

where C_i and C_j are so called as the Cotes coefficients.

Substitute (16) into (11)-(13) yields the composite solutions for B_{+x}, B_{+y}, and B_{+z} by the combination of numerical integration and analytic derivation method. In a similar way, the mixed solutions for B_{-x}, B_{-y}, and B_{-z} can be evaluated. Thus, the complete semi-analytic expressions for the three components of magnetic flux density **B** at field point P produced by the axially-polarized cylindrical permanent magnet have been derived.

2.2. Output Voltage of Hall Sensor

According to Hall effect, the output voltage of a Hall sensor under magnetic field satisfies

$$U_H = \frac{R_H I_c}{d} B = R_H' B \quad (17)$$

where R_H, d and I_c are the Hall coefficient, thickness of the semiconductor slice, and the current flowed through Hall sensor, respectively; B is the effective magnetic flux density component applied on the Hall sensor. The B is shown in Fig. 1 and Fig. 2 referred to the perpendicular component of magnetic flux density **B** produced by the above mentioned permanent magnet.

As shown in Fig. 1 and Fig. 2, when a relative horizontal displacement ΔX, vertical displacement ΔZ and/or tilt angle θ_0 take place between Solenoid I and II, the relative geometrical position between the permanent magnet on the upper surface of Solenoid I and the Hall sensor on the lower surface of Solenoid II is changed, causing the effective magnetic flux density B applied on the Hall sensor and the Hall voltage generated on the studied Hall sensor to vary accordingly.

For the Hall voltage measuring circuit in the H-V type sensor, a high performance micro linear Hall sensor SS94A1 from the Honeywell Company is applied. The power supply voltage V_s for Hall sensor SS94A1 is 10 VDC. The output voltage of Hall sensor is connected to the A/D input pin of main control chip MSP430F155. According to the transmission performance of SS94A1, the zero voltage will reach 5 V when the supply voltage is 10 V, and the output Hall voltage will linearly change from 1.875 V to 8.125 V when the externally imposed magnetic field varies from -50 mT to 50 mT.

Denoting the effective magnetic flux density produced by the permanent magnet on the Hall sensing surface as B_e, which has a specific functional relationship with the magnet geometry and the relative geometrical position between Solenoid I and II. As shown in Fig. 1 and Fig. 2, when the horizontal distance X_1 and vertical distance Z_1 between the center of the Hall sensing surface and that of the magnet lower surface is fixed with relations $X_1=\Delta X$ and $Z_1=Z_0+\Delta Z$, the cylindrical coordinate of sensing surface's center point P′ can be expressed as $P'(\rho,\varphi,z)=P'(X_1,0,Z_1)$, which is then used for coordinate substitution for the field point P in the above presented Hall voltage measurement model, and after further execution of the semi-analytic solving approach characterized by mixing the equivalent magnetic charge model with the 2-D numerical integral method, B_e can be calculated quantitatively.

Eqs. (4)-(13) show that the magnetic flux density **B** at the observation point P′ outside the cylindrical magnet has three directional components, B_x, B_y, and B_z. However, according to working principle of the hall sensor, only the component normal to the Hall magnetic surface can effectively excite Hall effect, which is denoted as B_e. As shown in Fig. 1, when Solenoid I and II are arranged in coaxial or parallel-axial state, $B_e=B_z$. When these two solenoids are in cross-axial state with a axial tilt angle θ_0, B_e is given by

$$B_e = B_z \cos\theta_0 - B_x \sin\theta_0 \tag{18}$$

2.3. Setup of Hall Voltage Measuring Model

The relationship between B_e and U_H is varied with performance of the Hall sensor and gain of the amplifying module. After analysis on the I/O characteristic of our proposed Hall voltage measuring circuit and the sensing feature of Hall sensor SS94A1, the sensitivity of Hall voltage can be deduced by

$$S_H = \frac{\Delta V}{\Delta B} = \frac{6.25V}{0.1T} = 62.5\,(\mathrm{V/T}) \tag{19}$$

So there is a linear relationship between B_e and U_H as follows,

$$U_H = S_H B_e \tag{20}$$

3. Experiments and Model Verifications

3.1. Experiment Setup and Procedure

For an objective and credible evaluation of Hall sensing characters of the proposed H-V type sensor and of performance of EMC-NI model in characterizing the complex functional relationship among the sensor's Hall voltage output U_H, the parameters to be measured including the relative horizontal displacement ΔX, vertical displacement ΔZ and tilt angle θ_0, and its geometry and shape parameters, a series of Hall voltage measuring experiments are conducted and the measuring results are carefully studied and compared with the simulation results based on EMC-NI model. Experiments were conducted on the underground displacement measurement test platform built at the Geological Disaster Monitoring Equipment Research center in China Jiliang University [8]. As shown in Fig. 3, the experiment setup mainly consists of three parts:

1) Prototype of the H-V type sensor, mainly composing of two adjacent integrated sensor units named as Solenoid I and Solenoid II respectively;

2) 4-axis joint drive unit and controller for underground displacement measurement that can continuously adjust the relative horizontal displacement ΔX, vertical displacement ΔZ and tilt angle θ_0 between Solenoid I and II; 3) SCM control system which can achieve an automatic measurement and recording of such measuring parameters as ΔX, ΔZ and θ_0 between these two solenoids and the Hall voltage U_H output by the Hall voltage measuring circuit.

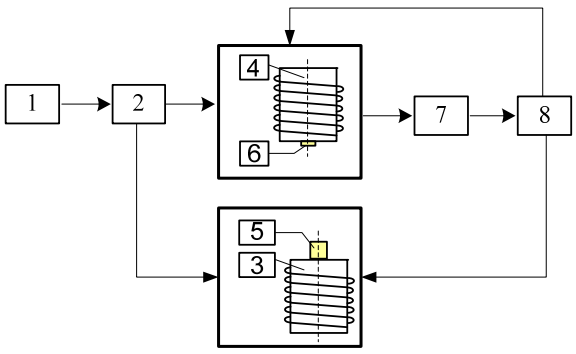

Fig. 3. Schematic diagram of the experimental setup. 1-4 axial joint drive controller; 2-4 axial joint drive unit; 3-Solenoid I and sensing integrated circuit embedded in its inner wall; 4-Solenoid II and sensing integrated circuit embedded in its inner wall; 5-Permanent magnet; 6-Hall sensor; 7-Hall voltage measuring circuit; 8-SCM control system.

The scheme for Hall voltage measuring experiments and modeling simulations are illustrated in Fig. 4. Before the experiment, we arrange the center of permanent magnet lower surface and center of Hall sensor sensing surface in the same vertical

line, namely the initial horizontal distance X_0 equal to zero, and set their initial vertical distance Z_0 to some fixed value. During the experiment, we move the Hall sensor in x or z direction to change its relative horizontal displacement ΔX or vertical displacement ΔZ, and rotate its magnetic sensing surface to change the relative axial tilt angle θ_0. Under such conditions, the corresponding output values of Hall voltage are recorded and compared with the EMC-NI theoretical simulation results so as to test the sensor's Hall property and EMC-NI modeling accuracy on the counterpart geometry and material characteristic configuration for the H-V type sensor as listed in Table 1 and Table 2. The initial vertical distance Z_0 between the magnet and Hall sensor is selected as 33 mm, and the variation ranges of ΔX and ΔZ are both 30 mm.

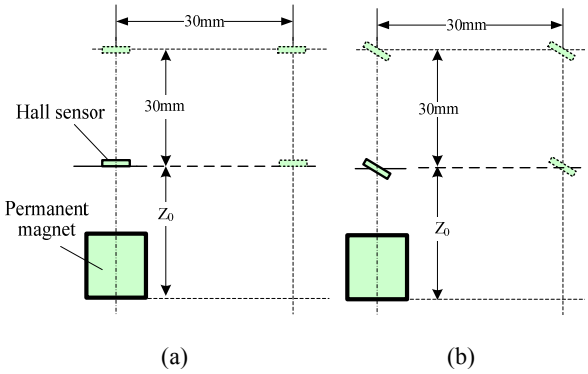

Fig. 4. Experiment and simulation scheme for Hall voltage measurement with tilt angle (a) θ_0=0 and (b) $\theta_0 \neq 0$.

Table 2. Geometrical Parameters of Solenoid I and II.

Parameter	Unit	Value	Comment
Diameter (d)	mm	70	
Length (a)	mm	75	
Coil turns (w)	turn	400	divided by 3 layers
Initial Z_0	mm	33	

3.2. Experiments and Model Validations

Fig. 5 plots 3-D graphs of the experimentally measured and EMC-NI modeled Hall voltage *versus* the simultaneous variations of ΔX and ΔZ under some fixed tilt angles θ_0. It can be seen, whenever θ_0 is 0° or 20°, the EMC-NI modeled 3-D graphs show quite high shape and value consistency to the measured 3-D graphs, thus initially proves the reliability and accuracy of EMC-NI model in formulation of Hall sensing properties of the H-V type sensor.

In order to directly display and compare point by point the measured and simulated results of Hall voltage when the horizontal displacement, vertical displacement and tilt angle are simultaneously changed, from Fig. 5 we can further extract some 2-D graphs by specifying the value of ΔX or ΔZ.

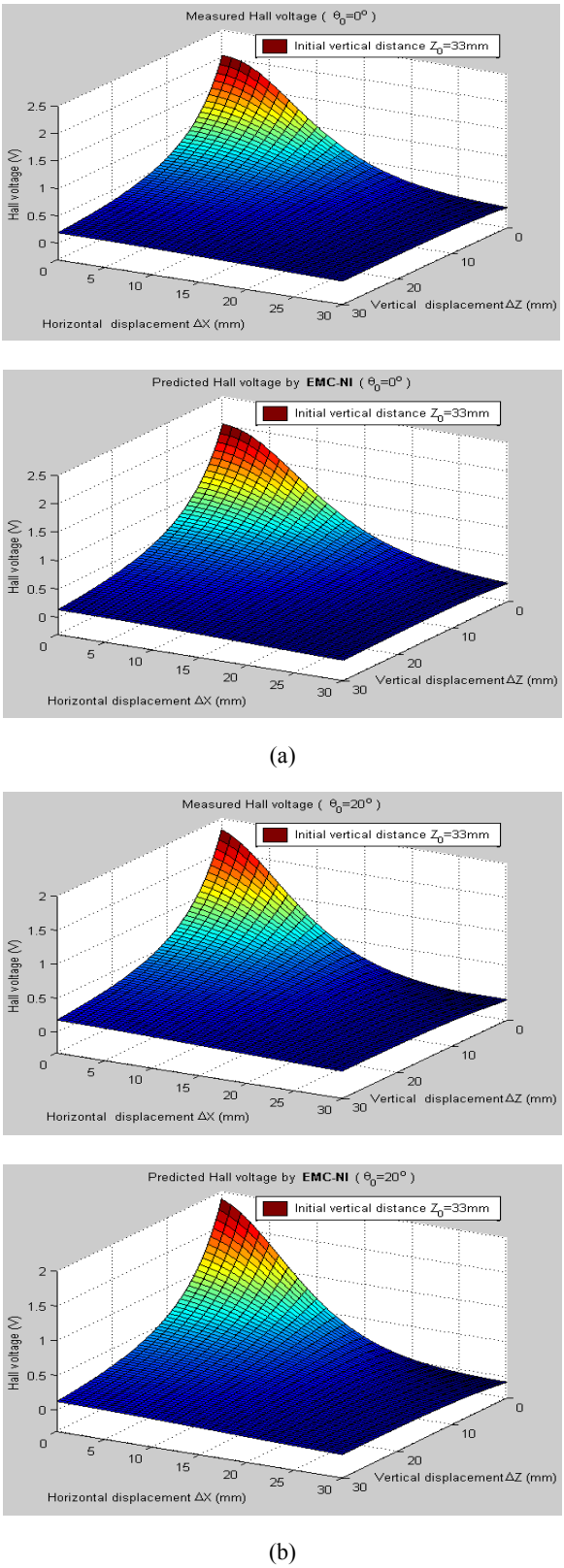

Fig. 5. 3-D graphs of measured Hall voltage and **EMC-NI** predicted Hall voltage *versus* variations of ΔX and ΔZ. (a) θ_0=0°, (b) θ_0=20°.

Fig. 6 and Fig. 7 show the corresponding 2-D graphs of the measured and predicted Hall voltage varied with ΔX when specifying the axial tilt angle as 0° and 20° respectively, and Fig. 8 and Fig. 9 are the

normalized curves based on Fig. 6 and Fig. 7 for further close-up analysis. It can be seen that, whether θ_0 equals 0° or 20°, and ΔZ equals 0 mm, 5 mm, 10 mm or 15 mm, the predicted Hall voltage and the measured one always display the same variation trend with good curve fitness with respect of the continuous variations of ΔX. It is shown that even under such a stringent point to point spatial comparison, the modeled Hall voltage still shows good tracking of the measured Hall voltage with a small overall voltage amplitude deviation. And their normalized curves are almost overlapped.

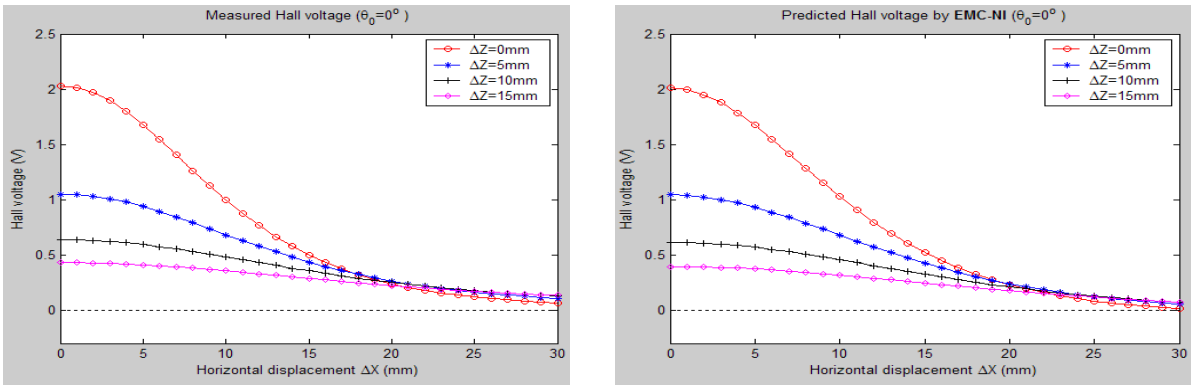

(a) (b)

Fig. 6. 2-D graphs of (a) measured and (b) **EMC-NI** predicted Hall voltage varied with ΔX when θ_0**=0°**.

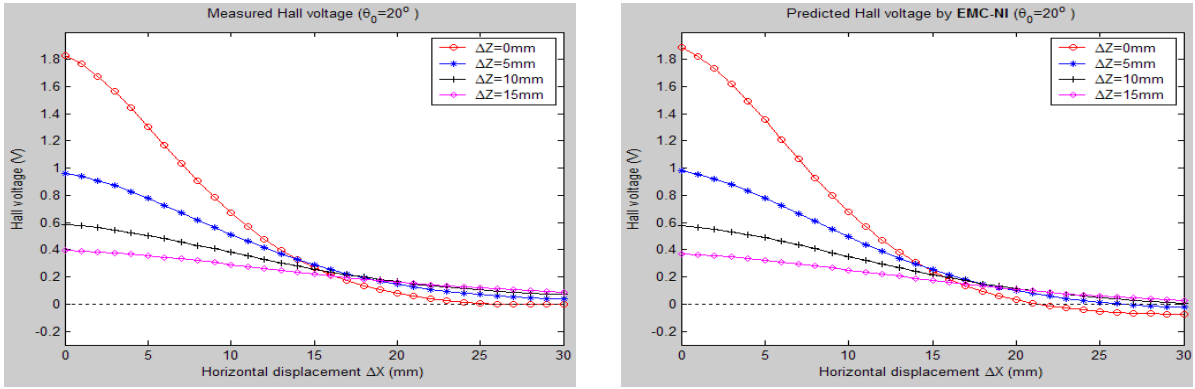

(a) (b)

Fig. 7. 2-D graphs of (a) measured and (b) **EMC-NI** predicted Hall voltage varied with ΔX whenθ_0**=20°**.

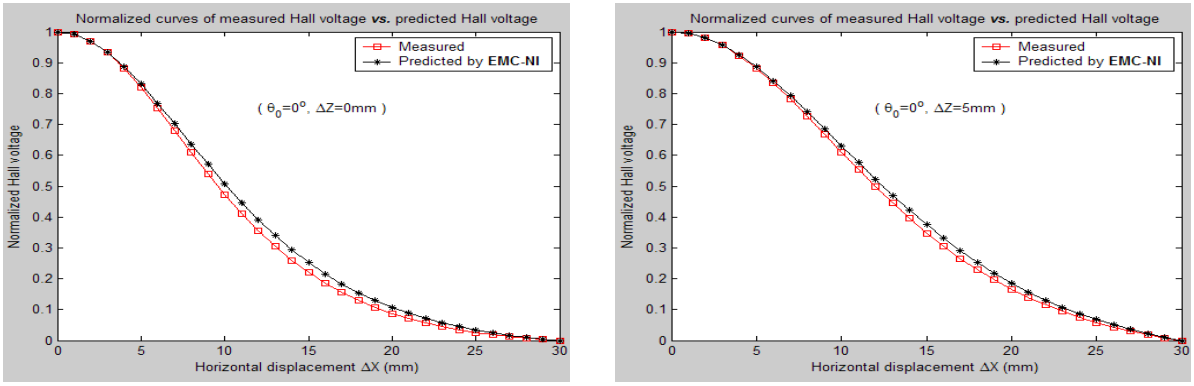

(a) (b)

Fig. 8 (a, b). Normalized curves for measured and **EMC-NI** predicted Hall voltage varied with ΔX when θ_0**=0°**.
(a) ΔZ=0 mm; (b) ΔZ=5 mm.

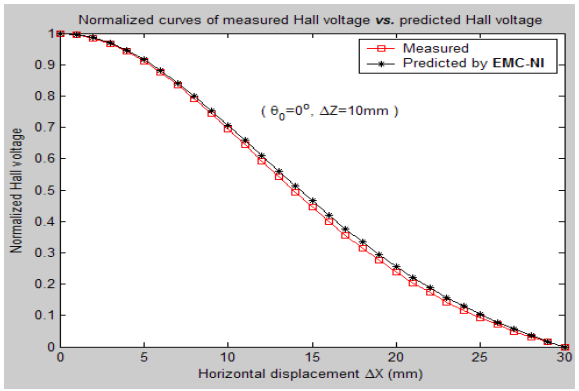

(c)

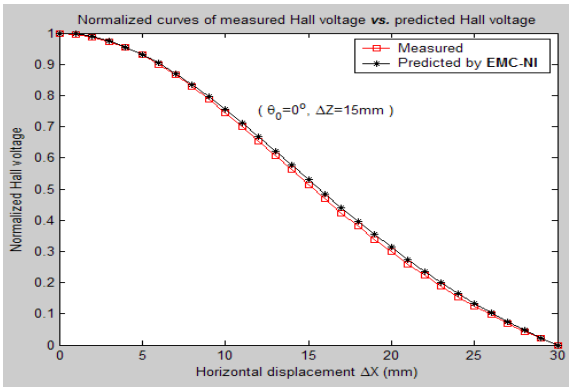

(d)

Fig. 8 (c, d). Normalized curves for measured and **EMC-NI** predicted Hall voltage varied with ΔX when θ_0**=0°**. (c) ΔZ=10 mm; (d) ΔZ=15 mm.

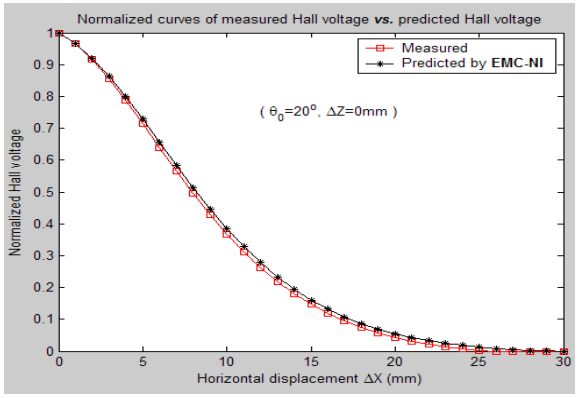

(a)

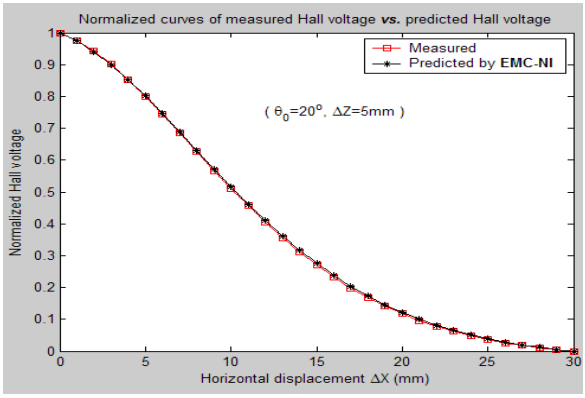

(b)

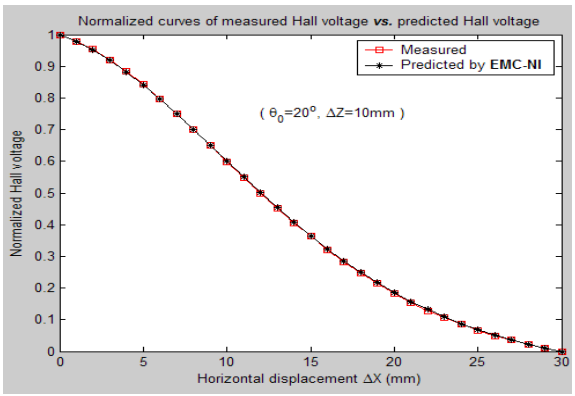

(c)

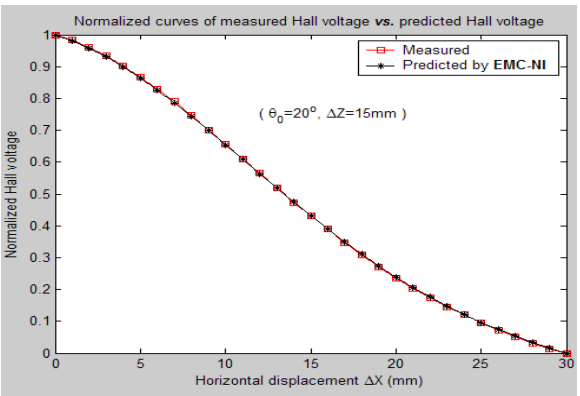

(d)

Fig. 9. Normalized curves for measured and **EMC-NI** predicted Hall voltage varied with ΔX when θ_0**=20°**. (a) ΔZ=0 mm; (b) ΔZ=5 mm; (c) ΔZ=10 mm; (d) ΔZ=15 mm.

In the same way, 2-D graphs of the measured and modeled Hall voltage *versus* vertical displacement ΔZ under different values of θ_0 and ΔX are plotted and studied. Some similar conclusions can be draw as follows: good shape consistency and amplitude approximation have achieved between the measured and simulated results along with variation of ΔZ whatever θ_0 is selected as 0° or 20°, and ΔX as 0 mm, 5 mm, 10 mm or 15 mm. Furthermore, in most cases their normalized curves are almost overlapped, thus displaying quite high change consistency between the measured and EMC-NI predicted Hall voltage.

In all, for our proposed H-V type underground displacement sensor, after a series of comprehensive studies between the experimentally measured Hall voltage and the theoretically calculated Hall voltage

based on EMC-NI model under different parameter variation conditions, some general conclusions can be drawn: No matter what relative tilt angle θ_0 between two solenoids in the H-V type sensor is selected, whether the 3-D graphs of the measured and EMC-NI predicted Hall voltage with respect to a simultaneous variations of ΔZ and ΔX, or the 2-D graphs and the related normalized curves of the measured Hall voltage and modeled Hall voltage varied only with ΔZ or ΔX, quite good shape similarity and value consistency have demonstrated, thereby, EMC-NI model is validated to be a quite accurate and reliable Hall voltage measuring model in characterizing the sensing property for the novel H-V type underground displacement sensor.

4. Conclusions

Underground displacement monitoring is an important means and research focus for the prediction and prevention of geological hazards and quality safety evaluation of geotechnical engineering projects. In our previous studies, a novel Horizontal-vertical composite type underground displacement sensor, i.e., the H-V type sensor, has been designed and a quite accurate and efficient mutual inductance measuring model (NIELA) was presented to depict quantitatively the functional relationship between the mutual inductance voltage output and the measuring parameters including the underground horizontal displacement, vertical displacement, and tilted angle.

Through integrated application of Hall sensing mechanism analysis, permanent magnet 3D magnetic field solution, and the multidimensional numerical calculation method, this paper presents a Hall voltage measurement model called the Equivalent Magnetic Charge-Numerical Integration Model (EMC-NI). It can quantitatively describe the relationship among the sensor's measuring underground horizontal displacement, vertical displacement and tilt angle, its Hall voltage output, the geometrical and shape parameter of the sensor units and permanent magnet. It has greatly reduced model calculation complexity by introducing the equivalent magnetic charge modeling idea and multidimensional numerical integration solution technology. Furthermore, the permanent magnet magnetic field calculation is mainly formed on the magnetic field analytic expression through rigorous formula derivation, which has safeguard the model's overall theoretical reliability and computing accuracy. A series of theoretical modeling simulations and comparative studies with the experimental output have been conducted, which fully verify the effectiveness and accuracy of EMC-NI in characterizing the Hall sensing properties for the H-V type underground displacement sensor. The couples of NIELA and EMC-NI models constitute the H-V type sensor's underground displacement measuring models.

Acknowledgements

This work is funded by Zhejiang Provincial Natural Science Foundation of China under Grant No. LQ13F010003, the National Natural Science Foundation of China (NSFC) of the Special Fund for Basic Research on Scientific Instruments under Grant 61027005, the NSFC General Project under Grant No. 51074146 and 41376111, and the National Science and Technology Support Plan of China under Grant No. 2012BAK10B05-3.

References

[1]. Y. Yin, H. Wang, Y. Gao, X. Li, Real-time monitoring and early warning of landslides at relocated Wushan Town, the Three Gorges Reservoir, *Landslides*, China, Vol. 7, Issue 3, 2010, pp. 339-349.

[2]. F. Wang, T. Okuno, T. Matsumoto, Deformation characteristics and influential factors for the giant Jinnosuke-dani landslide in the Haku-San Mountain area, *Landslides*, Japan, Vol. 4, Issue 1, 2007, pp. 19-31.

[3]. L. Picarelli, G. Urciuoli, M. Ramondini, L. Comegna, Main features of mudslides in tectonised highly fissured clay shales, *Landslides*, Vol. 2, Issue 1, 2005, pp. 15-30.

[4]. C. H. Dowding, K. M. O'Connor, Comparison of TDR and inclinometers for slope monitoring, *Geotechnical Special Publication,* Vol. 1, Issue 1, 2000, pp. 80-90.

[5]. R. Fanti, Slope instability of San Miniato hill (Florence, Italy): possible deformation patterns, *Landslides*, Vol. 3, Issue 4, 2006, pp. 323-330.

[6]. C. H. Dowding, M. L. Dussud, W. F. Kane, K. M. O'Connor, Monitoring Deformation in rock and soil with TDR sensor cables, *Geotechnical News*, Vol. 21, Issue 2, 2003, pp. 51-59.

[7]. J. Corominas, J. Moya, A. Lloret, J. A. Gili, M. G. Angeli, A. Pasuto, S. Silvano, Measurement of landslide displacements using a wire extensometer, *Engineering Geology*, Vol. 55, Issue 3, 200, pp. 149-166.

[8]. N. Shentu, H. Zhang, Q. Li, H. Zhou, R. Tong, X. Li, A Theoretical Model to Predict Both Horizontal Displacement and Vertical Displacement for Electromagnetic Induction-Based Deep Displacement Sensors, *Sensors*, Vol. 12, Issue 1, 2011, pp. 233-259.

[9]. L. Simeoni, L. Mongiovì, Inclinometer Monitoring of the Castelrotto Landslide in Italy, *Journal of Geotechnical & Geoenvironmental Engineering,* Vol. 133, Issue 6, 2007, pp. 653-666.

[10]. J. Singer, K. Thuro, U. Sambeth, Development of a continuous 3d-monitoring system for unstable slopes using time domain reflectometry, *Felsbau*, Vol. 24, Issue 3, 2006, pp. 16-23.

[11]. X Hou, X Yang, Q Huang, Using inclinometers to measure bridge deflection, *Journal of Bridge Engineering,* Vol. 10, Issue 5, 2005, pp. 564-569.

[12]. W. Weitschies, O. Kosch, H. Mönnikes, L. Trahms, Magnetic marker monitoring: an application of biomagnetic measurement instrumentation and principles for the determination of the gastrointestinal behavior of magnetically marked solid dosage forms, *Advanced Drug Delivery Reviews*, Vol. 57, Issue 8, 2005, pp. 1210-1222.

[13]. J. P. Selvaggi, S. Salon, O. M. Kwon, M. V. K. Chari, Calculating the external magnetic field from permanent magnets in permanent-magnet motors-an alternative method, *IEEE Transactions on Magnetics,* Vol. 40, Issue 5, 2004, pp. 3278-3285.

[14]. E. Paperno, P. Keisar, Three-dimensional magnetic tracking of biaxial sensors, *IEEE Transactions on Magnetics,* Vol. 40, Issue 3, 2004, pp. 1530-1536.

[15]. Z. H. Qian, R. S. Chen, FDTD analysis of magnetized plasma with arbitrary magnetic declination, *International Journal of Infrared and Millimeter Waves,* Vol. 28, Issue 2, 2007, pp. 157-167.

[16]. Y. L. Chen, R. Azzam, F. B. Zhang, The displacement computation and construction pre-control of a foundation pit in Shanghai utilizing FEM and intelligent methods, *Geotechnical & Geological Engineering*, Vol. 24, Issue 6, 2006, pp. 1781-1801.